VARIABILITY OF CLOUD COVER AND ITS RELATION TO SPRINGTIME SNOWMELT AND RUNOFF

Edwin Sumargo[1] and Daniel R. Cayan[1,2]

ABSTRACT

Much of the variability in water supply and an important part of the uncertainty in water supply forecasts are driven by the variability in solar insolation, which in turn is modulated by cloud cover. Here we investigate the space/time variability of cloud and incoming radiation and how it may affect snowmelt and streamflow. We use NASA/NOAA Geostationary Operational Environmental Satellite (GOES 9-11 and 15) albedo product (α) spanning from 1996 to 2012 during the daytime (8-16 PST) over the westernmost U.S. (25-50 °N, 113-130 °W) with 4-km spatial and 30-minute temporal resolutions. Only elevations above 800 meters are included to avoid contaminations from coastal marine and low stratus clouds. A translation of cloud albedo (α_{cloud}) to incoming surface radiation yields results that are well correlated with time series from surface radiometers at selected Sierra Nevada locations. Cloud albedo varies considerably from day to day, month to month, and even from year to year. To determine the most prominent spatial α_{cloud} patterns and their temporal variability, we conduct a Rotated Empirical Orthogonal Function/Principal Component (REOF/PC) analysis. The 5 leading REOFs account for ~66% of the total α_{cloud} variance. The leading REOF (~19%) covers portions of the Sierra Nevada and the Cascades and has a relatively high variance during the springtime, indicating its pertinence to snowmelt. During spring and early summer, these anomalous cloud patterns exhibit significant influence on snowmelt and runoff (R^2 > 30%), with anomalously high α_{cloud} producing lower snowmelt/runoff and vice versa. Correlations reveal a strong change in the response to incoming radiation of snowmelt and streamflow over the seasonal transition from winter-to-spring-to-summer. Dry years and wet years exhibit considerable difference in cloud amount and pattern, with lower overall springtime cloudiness in drier years, which leads to higher surface radiation available for snowmelt. (KEYWORDS: cloud variability, snowmelt, streamflow, satellite remote sensing, empirical orthogonal function)

INTRODUCTION

Springtime snowmelt and runoff are essential hydrologic processes in regions where most of the precipitation manifest as mountain snow during the winter months, such as in the western United States. A key factor that distinguishes such regions is the spring onset, when the streams "begin their seasonal flow pulse in response to melting of mountain snowpack" (Cayan et al., 2001). More recently Lundquist and Flint (2006) discovered that shading and solar radiation differences play a dominant role in the spring onset. These findings highlight previous studies, in which net solar radiation is found to be the primary energy input for spring snowmelt (U.S. Army Corps of Engineers, 1956) by providing 66-90% of the total energy available for snowmelt (Marks and Dozier, 1992; Cline, 1997). Understanding how solar irradiance input affects snowmelt and runoff processes remains a fundamental concern for hydrologic forecasters.

Solar insolation has been considered as a primary input in hydrologic/water supply forecast models. Hydrologic modelers have painstakingly tried to parameterize solar insolation in their models, such as by establishing temperature-irradiance relationship and solar radiation table in the Precipitation-Runoff Modeling System (PRMS, Leavesley et al., 1983; Markstrom et al., 2015). The difficulties of such efforts are due mainly to a couple of reasons:

1. High variability of cloud cover, which is the primary modulator of incoming solar radiation, and
2. Sparse surface radiometer observation networks.

The observation issue is specifically problematic in mountainous setting where any surface instruments are difficult to set up and maintain owing to the difficult access. Therefore, point measurements and transects lack the ability to comprehensively describe spatial-temporal variability in mountainous terrain (Gautier et al., 1980;

Paper presented Western Snow Conference 2015
[1] Scripps Institution of Oceanography, University of California San Diego, La Jolla, CA, 92037, esumargo@ucsd.edu
[2] United States Geological Survey, La Jolla, CA

Bales et al., 2006; Rittger et al., 2011). Consequently, satellite observation is an increasingly common method used to obtain radiation measurements (Jennings, 2000; Molotch et al. 2004; Bales et al., 2006).

The objective of this paper is to present the spatial-temporal variability of cloud cover using NASA/NOAA Geostationary Operational Environmental Satellite (GOES) remote sensing and to investigate the effect of this variability on springtime snowmelt and runoff. The effect of this variability on surface insolation and its representation on hydrologic models are not elaborated in this paper.

STUDY AREA

Our study area is the western conterminous United States. The region is characterized by clear seasonal climate pattern with warm and dry summer and cool and wet winter. The abundance of mountainous terrain results in ample snowpack accumulation in the winter. Mountain runoff derives from both rainfall and snowmelt, with rainfall runoff occurring immediately but with snowmelt runoff occurring at a relatively gradual pace, mostly within spring and early summer. As a consequence, the region's water supply relies substantially on spring-to-summer snowmelt-runoff (CADWR Bulletin 160-98; Cayan et al., 1998; Das et al., 2013) and is especially vulnerable to climate change (Stewart et al., 2004; Barnett et al., 2008; Pierce et al., 2008; Hidalgo et al. 2009; Das et al., 2009, 2011).

Numerous *in situ* hydroclimatic measurement efforts in the mountainous western U.S. have been carried out for decades, including USGS streamflow discharge networks (http://waterdata.usgs.gov/nwis/) that extend as far as to the early 20th century. More recent measurement networks include snow courses (e.g. USDA Snow Telemetry/SNOTEL, http://www.wcc.nrcs.usda.gov/snow/) and basin-scale stream stage measurement (e.g. Lundquist et al., 2003). In contrast, the use of satellite data to specifically study cloud variability and its hydrologic implications in the western U.S. has not been widely orchestrated (e.g. Simpson et al., 2004).

All things considered, the western U.S. and California in particular, are well suited for out research objective. Following the domain of our satellite dataset (see DATA AND PROCESSING), we define the western U.S. as the region within the conterminous United States spanning from 130°W to 113°W and 25°N to 50°N.

DATA AND PROCESSING

Geostationary Operational Environmental Satellite (GOES) Albedo Product

We employ GOES-West (9-11, 15) visible albedo product (α) to characterize spatial-temporal cloud variability. Our dataset spans from 1996 to 2012 and covers the westernmost conterminous U.S. (25°N - 50°N, 130°W - 113°W) with 4-km spatial resolution and 30-minute temporal resolution. The half-hourly α dataset during the daytime scene (8-16 PST) is time-aggregated into daily data. The effect of changing surface reflectance is subtracted from α using a clear-sky filtering operation (modified from Paech et al., 2009) to produce the cloud albedo component (α_{cloud}):

$$\alpha_{cloud}(t) = \alpha(t) - \alpha_{clear}(t) \quad [1]$$

$$\alpha_{clear}(t) = \min(\alpha(t - t_0):\alpha(t + t_0)); \text{ where } t_0 = 7 \text{ days in this study.} \quad [2]$$

The climatological seasonal cycle of α_{cloud} is estimated as an average of each calendar day's α_{cloud} over the 17 years of record and smoothed using 29-day centered (±14 days) moving average. Anomalies are formed by subtracting the daily climatological α_{cloud} from each day's actual α_{cloud}.

A low elevation mask is applied to GOES pixels with surface elevations less than 800 meters to avoid marine and low-level stratus clouds (Figure 1), which are unwanted because they may represent different mechanisms and processes than clouds over the higher elevation terrain. For this purpose we utilize gridded elevation data with 2-minute spatial resolution obtained from National Oceanic and Atmospheric Administration (NOAA) National Geophysical Data Center Geophysical Data System (NGDC GEODAS) Grid Translator Design-a-Grid website (http://www.ngdc.noaa.gov/mgg/gdas/gd_designagrid.html). The gridded elevation dataset is then interpolated to GOES pixels to identify low/high elevation pixels.

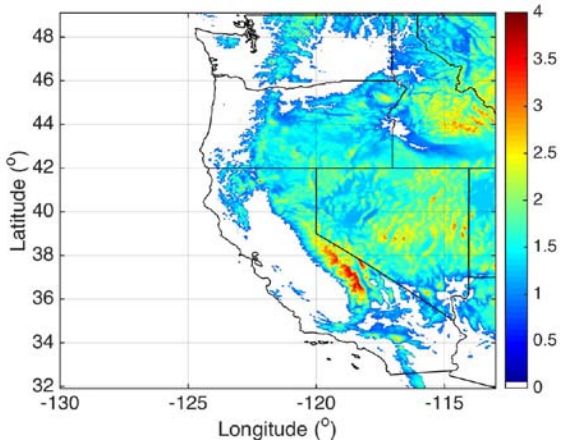

Figure 1. Surface elevation contour map (in km) showing the westernmost United States region with 800 m low-elevation mask corresponding to the domain of our GOES dataset. The state boundaries are obtained from http://maeresearch.ucsd.edu/kleissl/files/st99_d00_ascii.zip. The elevation dataset is obtained from NOAA NGDC GEODAS and interpolated to 4-km GOES pixels.

Snow Melt and Accumulation

Snow Water Equivalent (*SWE*) records are retrieved from United States Department of Agriculture (USDA) Natural Resources Conservation Service Snow Telemetry (NRCS SNOTEL, http://www.wcc.nrcs.usda.gov/snow/) and California Department of Water Resources (CADWR) Cooperative Snow Survey (tabulated on California Data Exchange Center/CDEC, http://cdec.water.ca.gov/) to further investigate snow response to cloud variability. Because snowmelt is the variable of interest, we define a simple proxy to snowmelt from *SWE*:

$$\Delta SWE(t) = SWE(t-1) - SWE(t+1) \quad [3]$$

such that $\Delta SWE > 0$ for melt and $\Delta SWE < 0$ for accumulation. ΔSWE is also de-seasonalized using smoothed (±14 day centered moving average) daily climatology in order to be consistent with α_{cloud}.

Stream Discharge

Stream discharge (*Q*) was obtained from United States Geological Survey (USGS, http://waterdata.usgs.gov/ca/nwis/) to investigate snowmelt-runoff response to cloud variability. The *Q* dataset for this study is the USGS Hydro-Climatic Data Network (HCDN) streamflow dataset, using a set of snowmelt-dominated gages identified by Stewart et al. (2005). Here we also define a simple streamflow term as the change in *Q* from the day before to the day after:

$$\Delta Q(t) = Q(t+1) - Q(t-1) \quad [4]$$

ΔQ is then de-seasonalized using smoothed (±14 day centered moving average) daily climatology in order to be consistent with α_{cloud} and ΔSWE.

METHODS

Rotated Empirical Orthogonal Function (REOF) Analysis of De-Seasonalized α_{cloud}

Rotated empirical orthogonal function (REOF) analysis is employed to identify a small set of patterns of cloud variability. Practically speaking, REOF analysis identifies clouds at different regions that vary in unison.

The Empirical Orthogonal Function (EOF) itself has been widely used to describe spatial and temporal meteorological, climate and oceanographic variability since its conception (Lorenz, 1956; Davis, 1976). However, it imposes a rigid spatial and temporal orthogonal constraint, which has been shown to produce spatial or temporal structures that may not be physically meaningful (Richman, 1986; Hannachi, 2004). One way to address this problem is to relax the orthogonal constraint by rotating its spatial component. Thus, we apply REOF method with Kaiser row normalization and varimax criterion (Kaiser, 1958) to describe spatial and temporal variability of de-seasonalized α_{cloud} over high-elevation domain in the westernmost U.S. for the whole year (Jan-Dec) between 1996 and 2012. We repeated the analysis for different periods, e.g. Feb-May, Jun-Sep, and Apr-Jul (not shown), and

found that only the first 5 REOF modes (amount to ~66% of the total variance) that vary seasonally (Figure 2). In this paper we exclusively evaluate the 2 leading modes.

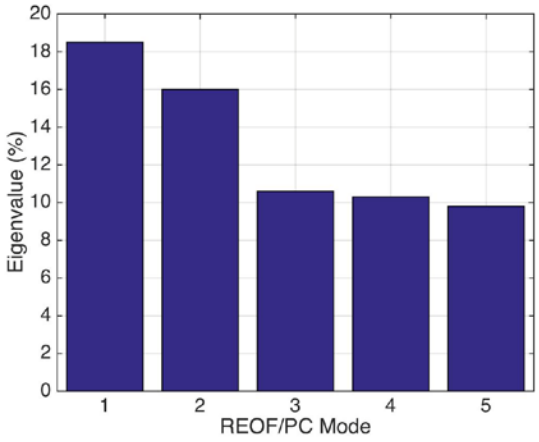

Figure 2. The eigenvalues associated with the first 5 REOF modes retrieved in this study, showing the percentage variances contributed by the 5 leading modes. The dominance of the 2 leading modes is particularly evident.

Simple Linear Regression Model of Snowmelt and Streamflow

The effect of cloud variability on springtime snowmelt (ΔSWE) and streamflow (ΔQ) is subsequently investigated. We construct multiple linear regression models of de-seasonalized daily ΔSWE and ΔQ for each month with 3 separate sets of predictors: PC-1, PC-2 and local/overhead α_{cloud}, and with each set consists of the predictors from day t – 5 to day t:

$$Y(t) = \Sigma\, C_n * X(t - n) \quad [5]$$

$$X = \text{PC-1, PC-2, local/overhead } \alpha_{cloud} \quad [5a]$$

$$Y = \Delta SWE, \Delta Q \quad [5b]$$

$$C_n = \text{regression coefficient, for } 0 \le n \le 5 \text{ days} \quad [5c]$$

Therefore, ΔSWE and ΔQ variations on one day are responses to PC-1, PC-2, and α_{cloud} variations from several preceding days. The effect of precipitation is neglected in this study. From these regressions we evaluate the lagged and cumulative responses of ΔSWE and ΔQ to α_{cloud} variations denoted as the squared Pearson's correlation coefficient (Pearson, 1895):

$$R^2 = \frac{[\sum_{i=1}^{n}(x_i-\bar{x})(y_i-\bar{y})]^2}{[\sum_{i=1}^{n}(x_i-\bar{x})^2][\sum_{i=1}^{n}(y_i-\bar{y})^2]} \quad [6]$$

where x and y are the same as X and Y in Equation [5].

RESULTS

Spatial and Temporal Characteristics of Mountain Cloud Variability in the Western U.S.

We retrieve and map the spatial component (REOF) of de-seasonalized α_{cloud} over high elevation domain in the westernmost U.S. to investigate the spatial structures of the 2 leading modes (REOF-1 and REOF-2, Figure 3). These modes amount to ~35% of the total variance, with the leading mode accounts for ~19%. The first mode is centered over the coastal ranges, the Sierra Nevada and extends to the South Cascades. The second mode is centered over the interior Pacific Northwest and parts of the Rocky Mountain in Idaho and Montana. Parts of the eastern Oregon are accentuated in both modes, which reflects the fact that these modes are not completely orthogonal.

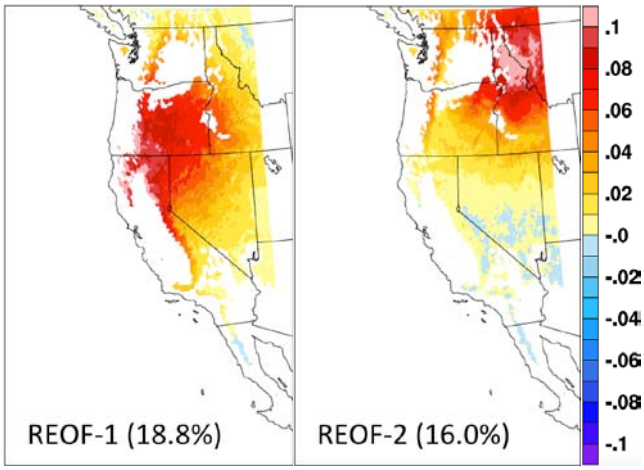

Figure 3. Maps of the 2 leading REOF modes, which account for ~35% of the total variance. The 1st mode is emphasized in the Sierra Nevada, South Cascade, and other Californian Pacific Coast ranges. The 2nd mode is emphasized in the northern Rockies and parts of Idaho and Montana. Warm colors (positive REOF) represent clouds, while cool colors (negative REOF) represent the lack

We also obtain the time component (Principal Component/PC) to investigate the seasonal patterns of the 2 leading modes (PC-1 and PC-2). Unlike the spatial component (REOF), the time component (PC) is not rotated and hence its modes are orthogonal to each other. The PC is a time-series of the amplitude of α_{cloud} fluctuation that appears noisy when plotted. As a way to describe this fluctuation, we evaluate the monthly sample standard deviations (σ) of both PC modes:

$$\sigma = \sqrt{\frac{1}{N-1}\sum_{i=1}^{N}(x_i - \bar{x})^2} \quad [7]$$

x = monthly aggregates of PC-1, PC-2 [7a]

N = length of PC-1, PC-2 time-series for that particular month [7b]

The result suggests that the leading mode has a high variability during the springtime, particularly between March and May, and a significantly lower variability during the summertime (Figure 4). On the other hand, the second mode is signified by high variability in late spring and early autumn, and by low variability in the mid-summer and winter.

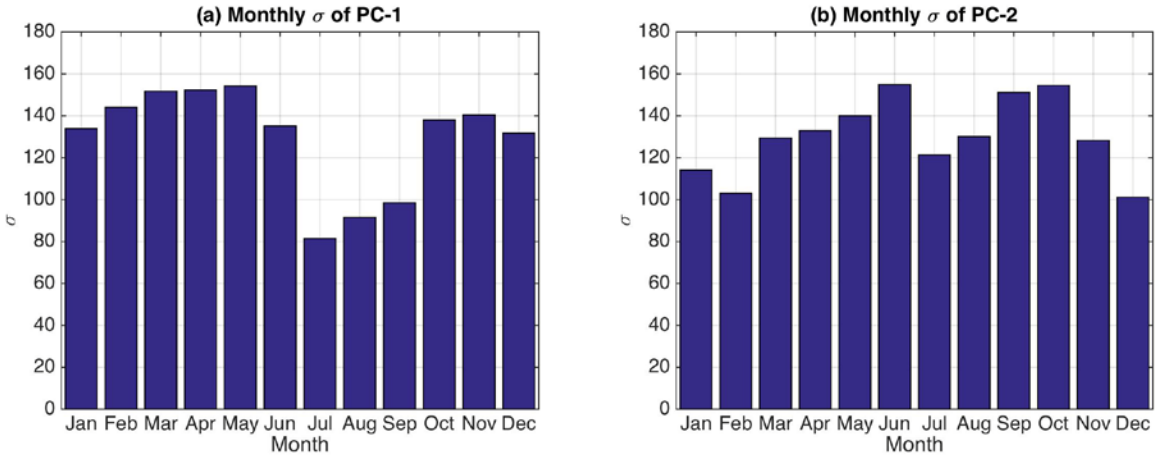

Figure 4. Monthly standard deviation (σ) of (a) PC-1 and (b) PC-2, illustrating seasonal importance of the 2 leading PC modes. The leading mode exhibits an annual cycle with particularly high variability in the spring, while the second mode shows a rather twice-yearly cycle with particularly high variability in the late spring and early autumn.

To sum up, the leading mode of α_{cloud} variability in the high elevation sites of the western U.S. is denoted by high variability in the Sierra Nevada and other Pacific Coast Ranges, while the second mode is concentrated in

the interior Pacific Northwest. Monthly σ of both PC-1 and PC-2 indicate relatively high variability in the spring, which suggest the importance of these modes of α_{cloud} variability for springtime snowmelt-runoff processes.

Inter-Annual Variability in Springtime Cloudiness

We form areal aggregates for each of the 2 leading REOF modes by identifying the pixels/regions with REOF values greater than a threshold value to investigate the inter-annual cloudiness variations associated with the 2 leading modes. In this case the threshold value is set to 0.06 (equivalent to the 76th percentile of REOF-1 and the 80th percentile of REOF-2). We determine Mar-May (MAM) to be the springtime period corresponding to the typical peak snowmelt season. Coefficient of variation is employed to exemplify the inter-annual α_{cloud} variability, which is described as the ratio of the standard deviation (σ) to the mean (μ) ($C_v = \sigma/\mu$).

The annual series of MAM α_{cloud} averages between 1996 and 2012 are plotted for REOF-1 and REOF-2 aggregates, and the coefficient of variation for each case is computed (Figure 5). We find that C_v is ~14% in REOF-1 case and ~10% in REOF-2 case. Yearly fluctuation is particularly evident in the 1st REOF case with lower α_{cloud} in drier years (i.e. years with early spring onsets), such as 2001 and 2007, and vice versa (~0.6 correlation with spring onset dates at Merced River at Happy Isles Bridge in Yosemite National Park, California).

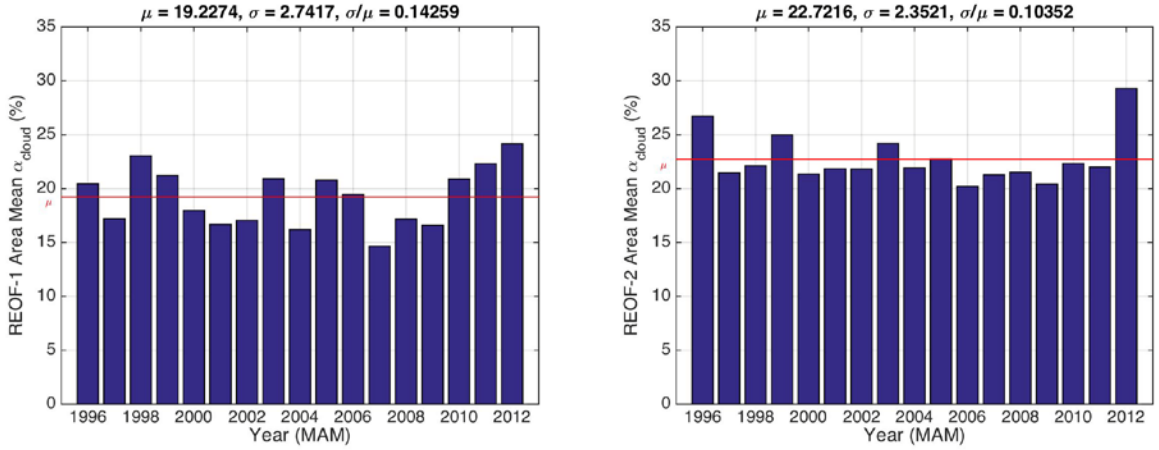

Figure 5. Annual time-series of MAM mean α_{cloud} between 1996 and 2012 averaged over REOF-1 (left) and REOF-2 (right) regions with REOF loadings greater than 0.06. The means (μ), standard deviations (σ) and the coefficients of variation ($C_v = \sigma/\mu$) of the time-series are computed. The red lines indicate μ.

We repeat C_v calculation on daily, weekly, and monthly basis for the REOF-1 areal aggregate. The days, weeks, and months that lie between March and May are identified, and the values of C_v corresponding to those days, weeks, and months are averaged. The resulting averages show that the inter-annual springtime α_{cloud} variability increases almost linearly as the time-scale/level is decreased from seasonal to daily (Table 1), which illustrate the influence of higher-frequency weather noise from monthly down to daily levels.

The trend observed in Table 1 is also observed when the averaging is segmented into individual months (March to June) instead of being lumped together from March to May (Table 2). The monthly averages of daily C_v come out as ~64% in March, ~67% in April, ~78% in May, and ~92% in June. The April, May and June C_v agree with what Simpson et al. (2004) reported for Merced and Carson River basins during 1999 alone.

Table 1. Mar-May mean coefficients of variation of α_{cloud} aggregated over areas with REOF-1 > 0.06 and computed from daily, weekly, monthly, and the whole seasonal (Mar-May) levels. The coefficient increases almost linearly with decreasing time-scale, reflecting the relative importance of high-frequency weather noise at lower time-scales.

Level	Daily	Weekly	Monthly	Seasonal
C_v (%)	69	42	22	14

Table 2. Same as Table 1, except C_v averaging is segmented into individual months (Mar-Jun) instead of the whole spring season (Mar-May).

Month/Level	Daily	Weekly	Monthly
Mar	64	40	23
Apr	67	37	15
May	78	53	28
Jun	92	52	29

Influence of Cloud Variability on Springtime Snowmelt and Runoff

The influence of cloud variability on snowmelt (ΔSWE) and runoff (ΔQ) is investigated. As an initial step, we perform monthly lead/lag correlation (R) between α_{cloud} and de-seasonalized ΔQ at Merced River at Happy Isles Bridge (HIB) in Yosemite National Park. The Dec-May segment is plotted below (Figure 6). The winter months (Dec-Feb) largely display positive R, which may suggest that the cloud variability is linked to precipitation event and in turn leads to rise in ΔQ. To the contrary, the spring months (Mar-May) exhibit the dominance of negative R, which suggest that ΔQ increases as α_{cloud} decreases and vice versa. This may indicate snowmelt-runoff mechanism in which clouds act as sunshade to the snowpack and as a result, less energy input for snowmelt-runoff occurrence.

More complicated pictures can be noticed at longer time lags in February, April and May. Negative R are observed at time lags greater than 1 day in January and February, while positive R are observed at time lags greater than 2 days in April and May. In February, for instance, a precipitating storm system in California produces rain at lower elevation sites including HIB (1,224 m), which is reflected by the positive R at shorter time lags. On the other hand, the same system is much more likely to deliver snowfall once making a landfall at higher elevation sites within the same basin, which in effect provides sunshade to the snowpack and hence results in a lower runoff at longer time lags downstream.

Later in April and May, a cloud system passing through California does not necessarily precipitate at lower elevation sites and consequently acts as a sunshade to the snowpack. Alternatively, the shading/non-shading effect may locally outweigh the precipitation effect on snowmelt. This cloud system may become orographically enhanced and produces precipitation as it moves farther upstream, which at this time of the year is more likely coming as rainfall that accelerates snowmelt and leads to a higher runoff downstream. (From a different perspective, the lack of clouds causes more solar energy reaching the surface and thus enhances local snowmelt and runoff. The lack of clouds farther upstream only leads to drying and a decline in streamflow downstream.)

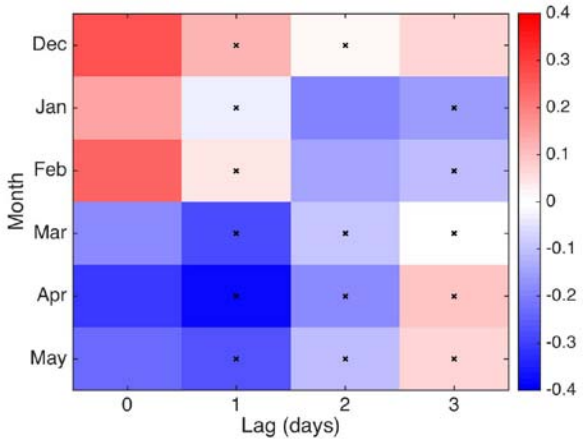

Figure 6. Dec-May lead/lag correlation between PC-1 and de-seasonalized runoff (ΔQ) recorded at Merced River at Happy Isles Bridge (HIB) in Yosemite National Park. ΔQ is de-seasonalized in the same way as α_{cloud} in order to be consistent with PC-1 (see METHODS). PC-1 leads ΔQ for lags > 0. 'x' denotes p-value < 0.05. The image displays negative ΔQ response to PC-1 with several day-lags during the peak snowmelt season (Mar-May).

To verify these conjectures, we set up a simple snowfall change proxy (Sf) from SWE measurement similar to Equation [3]:

$$Sf(t) = SWE(t + 1) - SWE(t - 1) \quad [8]$$

We pick *SWE* record from CADWR Tenaya Lake snow pillow (37.838 °N, 119.448 °W, 2,484 m), which is situated within Merced River basin. *Sf* is de-seasonalized using smoothed (±14 day centered moving average) daily climatology consistent with the PCs and Δ*Q*. We then lead/lag-correlate *Sf* with Δ*Q* in February and April of the same period as our GOES dataset (1996-2012). The results show similar behavior with positive correlations and followed by negative correlations in February and vice versa in April (Figure 7). The same behavior is also observed when we lag-correlate Δ*Q* to *Sf* derived from several other *SWE* measuring stations in Merced and the neighboring Tuolumne River basins (not shown).

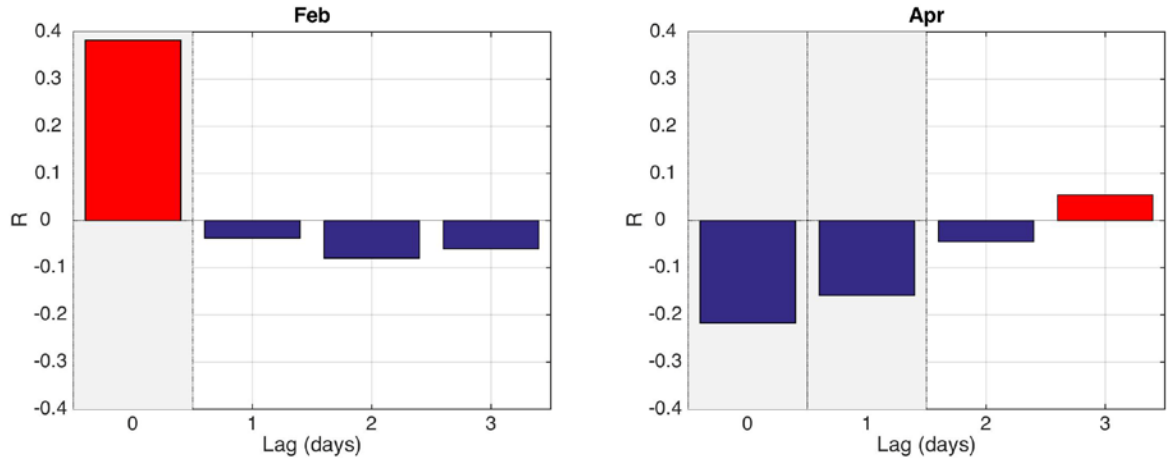

Figure 7. Lead/lag correlation between runoff (Δ*Q*) at USGS Merced River HIB and snowfall/accumulation proxy (*Sf*) at CADWR Tenaya Lake snow station in February (left) and April (right) of 1996-2012. *Sf* leads Δ*Q* for lags > 0. The gray shadings denote p-values < 0.05.

We hypothesize that the response of snowmelt-runoff to cloud variations spreads throughout several days. We then expand our analysis by obtaining *SWE* and *Q* from various snow stations and stream gages throughout the western U.S. corresponding to the domain of our GOES dataset. In doing so we define simple snowmelt and streamflow proxies (see DATA AND PROCESSING) and construct multiple regression models of snowmelt (Δ*SWE*) and streamflow (Δ*Q*) using PC-1, PC-2 and local/overhead α_{cloud} as 3 separate predictors to evaluate the cumulative response of snowmelt-runoff to cloud variations (see METHODS). The modeled Δ*SWE* and Δ*Q* are correlated to the corresponding predictor and the results are mapped (Figure 8).

The resulting maps show the distributions of the strength and lagged responses of Δ*SWE* and Δ*Q* to PC-1, PC-2, and local/overhead α_{cloud}. The response of Δ*SWE* is almost uniformly negative peaking at 0-2 day-lags with noticeable emphases in the Sierra Nevada and South Cascades for PC-1 and overhead α_{cloud}, and in the Cascades and other interior northwestern regions for PC-2. Rather mixed patterns are seen from the response of Δ*Q*, which largely shows negative response with 0-1 day-lag in the Sierra Nevada and South Cascades for PC-1 and overhead α_{cloud}, and nearly in all regions for PC-2. These patterns are in overall agreement with the regions where REOF-1 and REOF-2 are accentuated and exhibit sizeable responses with $R^2 > 30\%$.

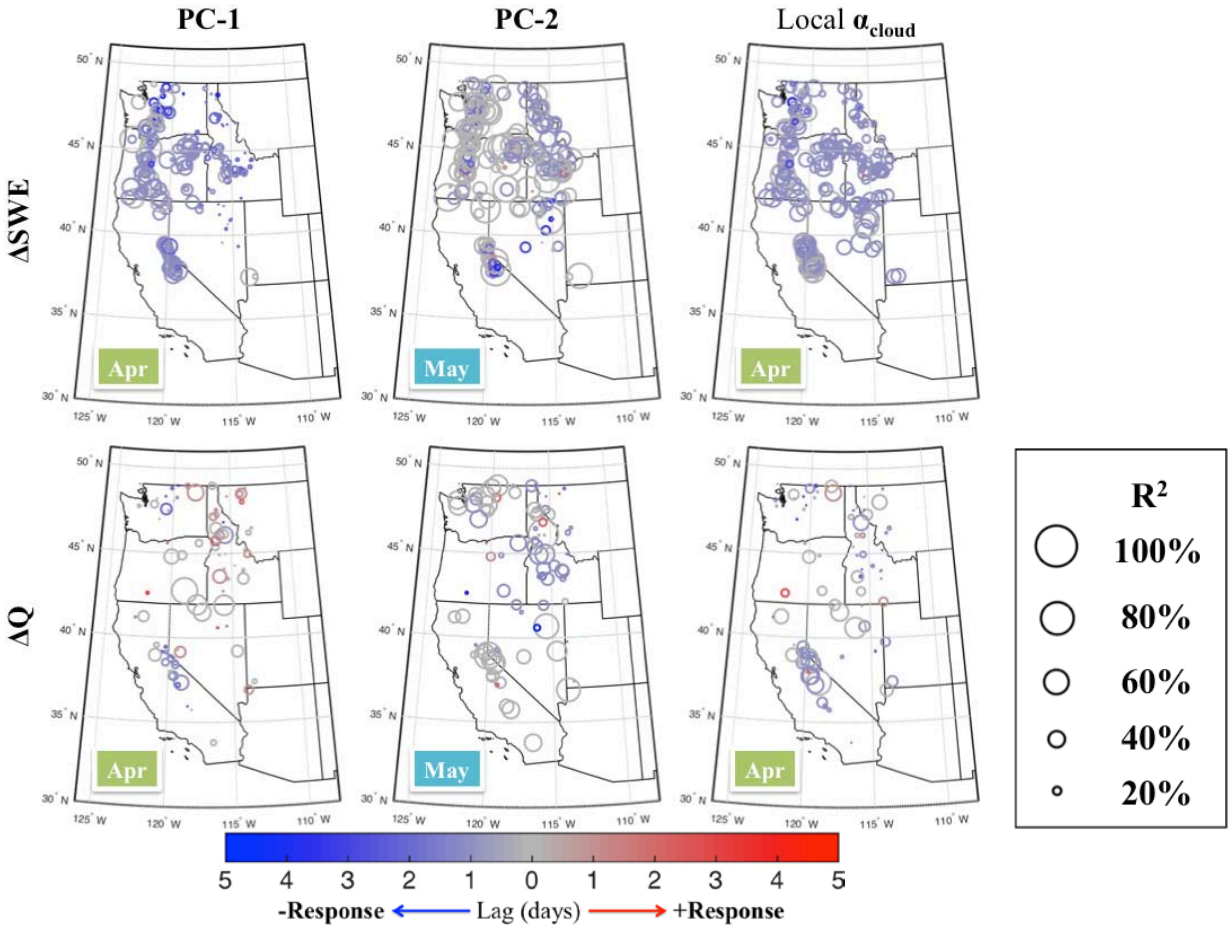

Figure 8. Maps showing snowmelt/Δ*SWE* (top) and streamflow/Δ*Q* (bottom) responses to PC-1 (left), PC-2 (center), and local/overhead cloud albedo/α_{cloud} (right) across the westernmost U.S. corresponding to the domain of our GOES dataset. Only results with at least 10 years of data and p-values < 0.05 are plotted. The size of the circles is proportional to R^2, which indicates the strength of the response. The colors indicate the peak day of the response based on the magnitudes of the regression coefficients, with blue represents negative response and red represents positive response. The choice of the months (April/May) corresponds to the months in which the responses are strongest for each set.

SUMMARY AND CONCLUSION

Understanding the variability of surface radiation is crucial for understanding processes and making accurate hydrologic forecasts in regions with mountain snowmelt and runoff, such as the western United States. Much of the uncertainties in surface radiation arise from the variation of cloud cover, which is incompletely described and not so well understood.

Our analysis reveal that the dominant mode of mountain cloud variability in the western United States accounts for 19% of the total variance, encompasses the Sierra Nevada and other Pacific Coast ranges, and is active during spring and early summer when snowmelt is peaking. These results highlight the importance of mountain cloud variability in regulating surface radiation budget during the snowmelt season in the westernmost U.S. What is more, the inter-annual variation of springtime (Mar-May) cloudiness amounts 14%, with lower overall cloudiness in dry years and vice versa.

The influence of cloudiness variability on springtime snowmelt/runoff is also investigated. We found that snowmelt and streamflow responses to cloudiness variability span over a few to several days, typically peaking 0 to 2 days after the onset of the responses. When calculated locally, cloud variations account for more than 30% of the

snowmelt and streamflow anomalies over most of the western U.S. The lagged responses are consistent with Lundquist et al. (2005) finding on the impact of basin's snow depth and heterogeneity on snow-fed streamflow timing.

ACKNOWLEDGEMENTS

We thank California Department of Water Resources (Contract #4600010378, AM-04) for providing support for Edwin Sumargo. We also thank NOAA RISA, California Energy Commission, and Southwest Climate Science Center for providing support for Daniel R. Cayan.

REFERENCES

Bales, R. C., N. P. Molotch, T. H. Painter, M. D. Dettinger, R. Rice, and J. Dozier. 2006. Mountain hydrology of the western United States. *Water Resources Research*, **42**(8).

Barnett, T. P., D. W. Pierce, H. G. Hidalgo, C. Bonfils, B. D. Santer, T. Das, G. Bala, A. W. Wood, T. Nozawa, A. A. Mirin, D. R. Cayan and M. D. Dettinger. 2008. Human-induced changes in the hydrology of the western United States. *Science*, **319**, 1080–1083.

California Department of Water Resources. 1998. Bulletin 160-98, http://www.waterplan.water.ca.gov/previous/b160-98/TOC.cfm.

Cayan, D. R., S. Kammerdiener, M. D. Dettinger, J. M. Caprio, and D. H. Peterson. 2001. Changes in the onset of spring in the western United States. *Bulletin of the American Meteorological Society*, **82**(3), 399-415.

Cayan, D. R., M. D. Dettinger, H. F. Diaz, and N. E. Graham. 1998. Decadal variability of precipitation over western North America. *Journal of Climate*, **11**, 3148-3166.

Cline, D. W. 1997. Snow surface energy exchanges and snowmelt at a continental, midlatitude Alpine site. *Water Resources Research*, **33**(4), 689-701.

Das, T., D. W. Pierce, D. R. Cayan, J. A. Vano and D. P. Lettenmaier. 2011. The importance of warm season warming to western U.S. streamflow changes. *Geophysical Research Letter*, **38**, L23403. doi:10.1029/2011GL049660.

Das, T., E. P. Maurer, D. W. Pierce, M. D. Dettinger, and D. R. Cayan. 2013. Increases in flood magnitudes in California under warming climates. *Journal of Hydrology*, **501**, 101-110.

Das, T., H. G. Hidalgo, D. R. Cayan, M. D. Dettinger, D. W. Pierce, C. Bonfils, T. P. Barnett, G. Bala and A. Mirin. 2009. Structure and detectability of trends in hydrological measures over the western United States. *Journal of Hydrometeorlogy*, **10**(4), 871-892.

Davis, R. E., 1976: Predictability of Sea Surface Temperature and Sea Level Pressure Anomalies over the North Pacific Ocean. *Journal of Physical Oceanography*, **6**, 249–266. doi: http://dx.doi.org/10.1175/1520-0485(1976)006<0249:POSSTA>2.0.CO;2

Hannachi, A. 2004. A primer for EOF analysis of climate data, *Reading: University of Reading*.

Hidalgo, H. G., T. Das, M. D. Dettinger, D. R. Cayan, D. W. Pierce, T. P. Barnett, G. Bala, A. Mirin, A. W. Wood, C. Bonfils, B. D. Santer, and T. Nozawa. 2009. Detection and attribution of stream flow timing changes to climate change in the western United States. *Journal of Climate*, **22**(13), 3838-3855.

Jennings, M. D.. 2000. Gap analysis: concepts, methods, and recent results. *Landscape Ecology*, **15**, 5–20.

Kaiser, H. F. 1958. The varimax criterion for analytic rotation in factor analysis. *Psychometrika*, **23**, 187–200.

Leavesley, G. H., R. W. Lichty, B. M. Troutman, and L. G. Saindon. 1983. Precipitation-runoff modeling system: User's manual. *Water-Resources Investigation Report*, 83-4238 pp., U.S. Geol. Surv.

Lorenz, E. N. 1956. Empirical orthogonal functions and statistical weather prediction. Statistical Forecasting Project Rep. 1, MIT Department of Meteorology, 49 pp.

Lundquist, J. D., D. R. Cayan, and M. D. Dettinger. 2003. Meteorology and hydrology in Yosemite National Park: A sensor network application, in Information Processing in Sensor Networks, edited by F. Zhao and L. Guibas, IPSN 2003, LNCS 2634, 518 – 528.

Lundquist, J. D., M. D. Dettinger, and D. R. Cayan. 2005. Snow-fed streamflow timing at different basin scales: Case study of the Tuolumne River above Hetch Hetchy, Yosemite, California. *Water Resources Research,* **41,** W07005.

Marks, D., and J. Dozier. 1992. Climate and energy exchange at the snow surface in the alpine region of the Sierra Nevada: 2. Snow cover energy balance. *Water Resources Research*, **28**(11), 3043-3054.

Markstrom, S. L., R. S. Regan, L. E. Hay, R. J. Viger, R. M. T. Webb, R. A. Payn, and J. H. LaFontaine. 2015. PRMS-IV, the precipitation-runoff modeling system, version 4. *U.S. Geological Survey Techniques and Methods*, book 6, chap. B7, 158 p., http://dx.doi.org/10.3133/tm6B7.

Molotch, N. P., T. H. Painter, R. C. Bales, and J. Dozier. 2004. Incorporating remotely sensed snow albedo into spatially distributed snowmelt modeling. *Geophysical Research Letter*, **31**, L03501, doi: 10.1029/2003GL019063.

Paech, S. J., J. R. Mecikalski, D. M. Sumner, C. S. Pathak, Q. Wu, S. Islam, and T. Sangoyomi. 2009. A calibrated, high-resolution GOES satellite solar insolation product for a climatology of Florida evapotranspiration. *Journal of the American Water Resources Association*, **45**(6), 1328–1342.

Pearson, K. 1895. Notes on regression and inheritance in the case of two parents. *Proc. R. Soc. Lond.*, **58**, 240-242.

Pierce, D. W., T. P. Barnett, H. G. Hidalgo, T. Das, C. Bonfils, B. D. Santer, G. Bala, M. D. Dettinger, D. R. Cayan, A. Mirin, A. W. Wood, and T. Nozawa. 2008. Attribution of declining western US snowpack to human effects. *Journal of Climate*, **21**(23), 6425-6444.

Richman, M. B. 1986. Rotation of principal components. *Journal of Climate*, **6**(3), 293-335.

Rittger, K., A. Kahl, and J. Dozier. 2011. Topographic distribution of snow water equivalent in the Sierra Nevada, paper presented at the 2011 Western Snow Conference, Lake Tahoe, Nev., 18-22 April.

Simpson, J. J., M. D. Dettinger, F. Gehrke, T. J. McIntire, and G. L. Hufford. 2004. Hydrologic scales, cloud variability, remote sensing, and models: Implications for forecasting snowmelt and streamflow. *Weather and forecasting*, **19**(2), 251-276.

Stewart, I., D. R. Cayan, and M. D. Dettinger. 2004. Changes in snowmelt runoff timing in western North America under a 'Business as Usual' climate change scenario. *Climatic Change*, **62**(1), 217-232.

Stewart, I. T., D. R. Cayan, and M. D. Dettinger. 2005. Changes towards earlier streamflow timing across western North America. *Journal of Climate*, **18**, 1136-1155.

U.S. Army Corps of Engineers. 1956. Snow hydrology: Summary report of the snow investigations. North Pacific Division, U.S. Army Corps of Engineers, 437 pp.